Efficient Energy Dissipating Steel-Braced Frame to Resist Seismic Loads

Murat Dicleli, M.ASCE[1]; and Anshu Mehta[2]

Abstract: In this research, the seismic performance of a proposed efficient energy dissipating steel-braced frame (EEDBF) in relation to that of a moment-resisting frame (MRF) and chevron braced frame (CBF) is studied. The frame is intended to combine the advantages of MRF and CBF and eliminate most of the disadvantages pertinent to these frames. Nonlinear static pushover, time history, and damage analyses of the three frames are conducted to assess the performance of the EEDBF compared to that of MRF and CBF. The analyses results revealed that the EEDBF has a more stable lateral force-deformation behavior compared to CBF. The energy dissipation capacity of the EEDBF is comparable to that of the MRF. The drift of the EEDBF at small to medium intensity ground motions is comparable to that of the CBF and smaller than that of the MRF. At high intensity ground motions, the drift of the EEDBF is smaller than those of both CBF and MRF. Furthermore, the EEDBF is found to experience less damage compared to other frames.

DOI: 10.1061/(ASCE)0733-9445(2007)133:7(969)

CE Database subject headings: Seismic effects; Energy dissipation; Steel frames; Bracing; Damage.

Introduction

Steel structures are designed for ductility, where the earthquake input energy is dissipated in plastic hinges that occur in frame members. The purpose of such a design is to enforce a ductile mechanism to form without permitting the structure to collapse. However, yielding of the plasticized zones and the resulting large permanent displacements induced by strong earthquakes may be so severe that nearly irreparable damage to conventional steel structural systems, such as moment-resisting frame (MRF) and/or chevron braced frame (CBF), is possible under this design philosophy. Thus, it may be required to rebuild the essential structural members of the structure following a strong earthquake to ensure a satisfactory performance under service loads.

MRF and CBF are commonly used in the construction of steel buildings. The MRF has a large ductility capacity compared to other frame types. However, the ductility demand is highly sensitive to the magnitude of the gravity loads (Park et al. 1997). Moreover, a MRF requires large member sizes to keep the lateral drifts within code-mandated limits (Bruneau et al. 1998). In an MRF, as the inelastic deformation of beams results in the dissipation of energy (Della Corte et al. 2002), substantive damage to these gravity load carrying members may be induced. Additionally, the flexibility of the MRF may result in large drift-induced nonstructural damage under seismic loading. Consequently, costly postearthquake rehabilitation of the structure may be required. On the other hand, CBF possesses a high elastic stiffness to prevent large drifts. Material saving could also be achieved as the frame members are subjected to less bending effect due to the presence of the braces (Gwozdoz and Machowski 1997). However, its ability to dissipate energy solely depends on the unstable hysteretic behavior of the braces due to buckling effects producing a loss of lateral stiffness and strength of the frame (Khatib et al. 1988). Thus, the response of the CBF is highly sensitive to the compactness and relative axial strengths of the braces in compression and tension (Redwood and Channagiri 1991; Georgesco et al. 1992) and the stiffness and strength of the beam into which the braces frame (Roeder 1989; Rai and Goel 2003). Furthermore, it is difficult to achieve a well-distributed ductility along the height of the CBF due to the premature buckling of the braces (Perotti and Scarlassara 1991) resulting in soft-story formations, dynamic instability (Tremblay 2001), and hence substantial damage to the frame members.

In light of the above discussion, it is clear that in addition to the advantages of each frame type, there are numerous disadvantages. Furthermore, both frames are prone to substantial structural damage during a strong earthquake. Consequently, a novel frame system with a design philosophy that will concentrate on minimizing seismic damage to the essential structural members of the frame is needed to ensure satisfactory postearthquake performance of steel buildings under service loads with minimal rehabilitation cost.

Proposed Efficient Energy Dissipating Steel-Braced Frame

The present research study is focused on a proposed efficient energy dissipating braced frame (EEDBF), configured to minimize seismic damage to its essential structural members by combining the advantages and eliminating most of the disadvantages of MRF and CBF. It is composed of a rigid frame with chevron

[1]Associate Professor and Vice Chair, Dept. of Engineering Sciences, Middle East Technical Univ., 06531 Ankara, Turkey. E-mail: mdicleli@metu.edu.tr

[2]Graduate Research Assistant, Dept. of Civil Engineering and Construction, Bradley Univ., Peoria, Illinois 61625.

Note. Associate Editor: Scott A. Civjan. Discussion open until December 1, 2007. Separate discussions must be submitted for individual papers. To extend the closing date by one month, a written request must be filed with the ASCE Managing Editor. The manuscript for this paper was submitted for review and possible publication on March 6, 2006; approved on December 14, 2006. This paper is part of the ***Journal of Structural Engineering***, Vol. 133, No. 7, July 1, 2007. ©ASCE, ISSN 0733-9445/2007/7-969–981/$25.00.

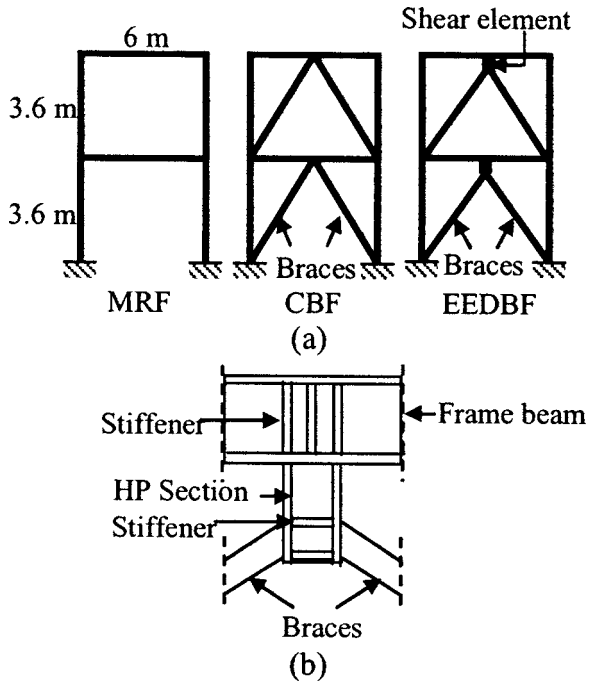

Fig. 1. (a) Typical two-story frames; (b) details of shear element and connections in EEDBF

braces and a conventional energy dissipating shear element (SE) connected between the braces and the beam as shown in Figs. 1(a and b). The SE is designed to yield in shear under the effect of the horizontal components of the brace axial forces before the compression brace buckles. It is built using a compact steel HP section. HP sections are composed of stocky plates and are generally used for piles due to their ability to sustain high axial impact loads during pile driving. Accordingly, such sections are capable of undergoing large inelastic deformations, as was validated by an earlier research study (Dicleli and Albhaisi 2004). Furthermore, unlike the shear links in eccentrically braced frames (EBF), the SE in the EEDBF is free of axial load effects since the vertical components of equal compression and tension brace forces cancel out. The proposed EEDBF is intended to behave similarly to a CBF prior to yielding of the SE under small to moderate intensity earthquakes to minimize interstory drifts. Under large intensity earthquakes, the EEDBF is intended to combine properties such as the high lateral stiffness of the CBF and the energy dissipating capacity of the MRF combined with that of the SE to minimize seismic damage to the essential structural components of the frame. Several other new frame systems have also been found in the literature (Sam et al. 1995; Clark et al. 1999; Chen et al. 2001; Phocas and Pocanschi 2003). However, compared to these, the proposed EEDBF combines the following advantages; (1) the frame has a relatively high elastic stiffness to prevent large interstory drifts under small to moderate intensity earthquakes; (2) the energy dissipation mechanism of the frame is conventional to facilitate its design and construction by the engineering community at large; and (3) the SE is capable of dissipating most of the earthquake input energy with minimal damage to the essential structural components of the frame. Most of the damage is anticipated to occur within the SE, which may be replaced after a potential earthquake. In the subsequent sections, the performance of the proposed EEDBF will be assessed in comparison to those of the MRF and CBF under monotonic and seismic loading.

Research Outline

In the first step of the research study, a summary of cyclic tests of shear links available in the literature is presented, and finite element simulation of the cyclic behavior of a typical shear link available in the literature is conducted using the program ADINA (2004) and compared with the test results to demonstrate that the behavior of the SE is simulated accurately. Then, a design strategy is adopted for the EEDBF to achieve a desired seismic behavior. Next, an analytical brace-buckling model is developed to simulate the inelastic cyclic behavior of the braces in CBF using the program ADINA (2004). The performance of the three frames is then studied in two phases considering sets of single- and multiple-story frames. In the first phase, extensive nonlinear static pushover (NLSP) and nonlinear time history (NLTH) analyses of a set of single-story frames are conducted to comprehend the behavior of the EEDBF in relation to MRF and CBF as a function of various structural and ground motion parameters. In addition, the extent of plastic penetration into the members of the frames under seismic loading is investigated to explore the potential seismic damage to the single-story EEDBF in comparison to MRF and CBF. In the second phase, the research is expanded to multiple-story frames. NLSP and NLTH analyses of two-; four-, and eight-story MRF, CBF, and EEDBF are conducted to assess the performance of the proposed EEDBF compared to those of the CBF and MRF. Next, seismic damage analyses of four-story MRF, CBF, and EEDBF are conducted to assess and compare the extent of potential damage in each frame.

Cyclic Behavior of SE

In the SE, the shear force created by the horizontal components of the EEDBF brace axial forces is constant along its length. This allows for the development of large plastic deformations without the development of excessive local strains as in the case of flexural yielding (Bruneau et al. 1998). Consequently, shear yielding provides a larger energy dissipation than flexural yielding (Kasai and Popov 1986a) and hence, it is adopted for the design of the SE in the EEDBF. Since the cyclic behavior of the SE forms an important part of the performance of the EEDBF, detailed information about the cyclic behavior of SE and its finite element simulation is given below.

Cyclic shear behavior of SE (or links) has been studied by many researchers. Hjelmstad and Popov (1983) conducted cyclic tests on short wide-flange SE used in EBF to study their cyclic behavior and energy dissipation capacity. It was found that a properly web-stiffened wide-flange SE is capable of producing a stable hysteretic behavior that leads to an efficient dissipation of energy. Hysteretic behavior of a properly stiffened SE (Specimen No. 4, size=W18$\times$40, length=711 mm) from the tests of Hjelmstad and Popov (1983) is demonstrated in Fig. 2(a). Kasai and Popov (1986b) studied the cyclic behavior of wide-flange SE with different lengths and axial forces. It was concluded that a SE with a properly stiffened web and even with unequal end moments can exhibit stable hysteretic behavior through large cyclic shear strains. More recently, McDaniel et al. (2003) performed cyclic tests on built-up wide-flange SE specimens for the new Oakland Bay Bridge to evaluate the link force and deformation capacities. The specimens behaved in a ductile manner until small cracks initiated at the end of the vertical fillet welds, connecting the intermediate stiffeners to the link web. A typical cyclic link shear force versus average plastic shear defor-

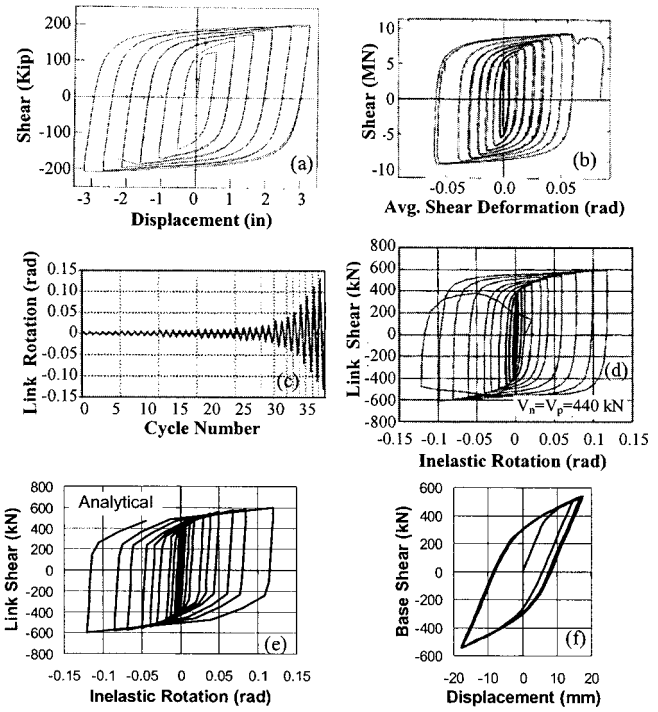

Fig. 2. (a) SE cyclic test results from Hjelmstad and Popov (ASCE 1983); (b) SE cyclic test results from McDaniel et al. (ASCE 2003); (c) shear rotation loading history for SE cyclic tests conducted by Okazaki et al. (ASCE 2005); (d) SE cyclic test results from Okazaki et al. (ASCE 2005); (e) finite element simulation of the SE cyclic test results from Okazaki et al. (ASCE 2005); and (f) cyclic base shear versus top displacement of single story EEDBF subjected to a harmonic (sine wave) ground acceleration

mation relationship obtained from these tests is demonstrated in Fig. 2(b). Okazaki et al. (2005) conducted a total of 23 tests to study the cyclic loading performance of SE in steel EBF. The shear rotation history used in the tests and the test results for one of the specimens (Specimen No. 4A-RLP, size=W10×33, length=684 mm) are demonstrated in Figs. 2(c and d), respectively. This test result also demonstrates a stable cyclic behavior for the SE and further proves the effectiveness of the SE for dissipating earthquake input energy in the proposed EEDBF.

To demonstrate that the behavior of the SE is simulated accurately in the NLTH analyses conducted as part of this research study, the finite element model of Specimen No. 4A-RLP tested by Okazaki et al. (2005) is built in ADINA (2004) and analyzed using cyclic pushover displacements calculated using the shear rotation history displayed in Fig. 2(c). Specimen No. 4A-RLP had a moment connection at both ends. However, the finite element model is built using a simple cantilever model with a length equal to the distance to the inflection point from one of the ends. The cyclic pushover displacement history used in the analyses is obtained by multiplying the cyclic shear rotations given in Fig. 2(c) by the length of the cantilever model. The analyses results are shown in Fig 2(e). A reasonably good agreement between the analytical and test results is obtained [Figs. 2(d and e)]. Fig. 2(f) demonstrates the NLTH analyses results of a single-story EEDBF subjected to a harmonic base excitation. The high postelastic stiffness of the curve displayed in Fig. 2(f) is due to the restoring effect of the elastic frame members (beam and columns are elastic, while the SE is yielding). The figure demonstrates that the analytical model of the SE used in the analyses also works well in NLTH analyses.

EEDBF Design Methodology

A design methodology based on preventing the buckling of the braces is adopted for the EEDBF to achieve a more stable lateral force-deformation behavior and to avoid damage to the braces and other structural members. The buckling of the braces is prevented by allowing the SE to yield in shear before the compression brace reaches its buckling capacity.

At the verge of the compression brace buckling, the axial tensile and compressive forces in the tension and compression braces will both be equal to the buckling load, P_b. Consequently, to prevent buckling of the compression brace, the SE is designed to have a plastic shear capacity, V_p, that is less than twice the horizontal component of the buckling load of the compression brace. Thus

$$\phi_o V_p \leq 2P_b \cos\theta \tag{1}$$

In the above equation, θ=angle that the chevron braces make with the horizontal; ϕ_o=overstrength factor to account for the variations in material strength and strain hardening effect for the SE; and V_p is expressed as (AISC 2001)

$$V_p = 0.6F_y d_w t_w \tag{2}$$

where F_y=yield strength of steel; and d_w and t_w=depth and thickness of the web. The ultimate failure mode for the SE is inelastic web shear buckling. To ensure a stable energy dissipation mechanism throughout the cyclic loading history of the EEDBF, this mode of failure may be delayed by the addition of web stiffeners. The required stiffener spacing, a, for various SE's rotation demands, γ_p, may be calculated using the following equation proposed by Kasai and Popov (1986b) for the shear links made of W sections in EBF

$$a = C_B t_w - 0.2d \tag{3}$$

where the constant C_B=56, 38, and 29, respectively for γ_p=0.03, 0.06, and 0.09 radians; and d=beam depth. However, as HP sections have stockier webs than those of W sections, and the configuration of the SE in the EEDBF is different than that of the link in EBF, the spacing requirement for the stiffeners may not be as strict. This needs to be verified experimentally.

Furthermore, the length, L_s, of the SE needs to be determined such that yielding occurs in shear before its plastic moment capacity, M_p, is reached. For the calculation of L_s, a rectangular V_p-M_p interaction is assumed based on the experimental test results of Kasai and Popov (1986a). Thus, neglecting the strain hardening effect, the length of the cantilever SE must be smaller than M_p/V_p to ensure shear yielding. However, due to the strain hardening effect, the SE's plastic base moment, M_p, and shear, V_p, may increase. The increase in M_p and V_p is accompanied by large flange strains that may result in premature failure of the welded SE-beam connection due to low cycle fatigue effects. {A bolted connection detail capable of developing shear yielding in the SE may be suggested to prevent such a failure and to facilitate the replacement of the SE after a potential earthquake. A typical bolted connection detail classified as fully restrained in FEMA 356 [Federal Emergency Management Agency (FEMA) 2000] may be used for this purpose (e.g., bolted end plate connection)}.

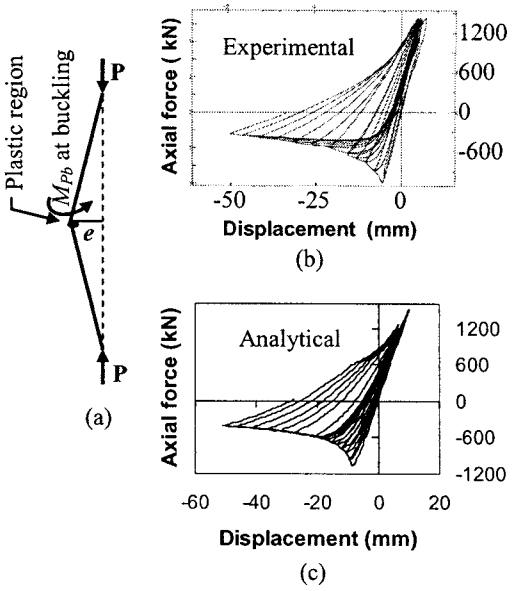

Fig. 3. (a) Nonlinear brace model; (b) experimental hysteresis loop (Black et al. 1980, reprinted with permission); and (c) analytical hysteresis loop generated by using ADINA (2004)

To prevent such a premature failure, an upper bound of $1.2M_p$ and a corresponding shear of $1.5V_p$ have been suggested by Kasai and Popov (1986a). Thus

$$L_s < \frac{1.2M_p}{1.5V_p} = \frac{0.8M_p}{V_p} \tag{4}$$

Designing the SE based on the above equations will ensure a more efficient energy dissipation based on shear rather than flexural yielding and a more satisfactory performance of the EEDBF without global buckling instability of the braces.

Analytical Modeling of Brace Inelastic Cyclic Behavior

In a CBF, principally the inelastic cyclic behavior of the braces results in the dissipation of earthquake energy. Hence, an accurate analytical simulation of this behavior including buckling effects is required in the analyses. For this purpose, an analytical brace model [Fig. 3(a)] is developed in ADINA (2004) to simulate the inelastic cyclic behavior of braces. An imperfection, e, is introduced at the center of the brace to produce a kinked element for simulating the global buckling effects using a large displacement analysis procedure. The imperfection, e, is given by the following equation (Dicleli and Mehta 2006):

$$e = \frac{M_{pb}}{P_b}\left(1 - \frac{P_b L^2}{12EI}\right) \tag{5}$$

where L, E, I, and M_{pb}=length, elastic modulus, moment of inertia, and plastic moment capacity of the brace at buckling load, respectively. The imperfection is calculated such that when the axial load reaches the buckling load, the plastic moment capacity is reached at the vertex of the kinked brace element due to second-order effects. Beyond this point, the axial load capacity of the brace constantly decreases due to the combined effects of increasing second-order moments and moment-axial force interaction as the member buckles. Accordingly, a plastic hinge region—accounting for moment-axial force interaction—is defined at the vertex of the kinked brace element using a set of axial-force-moment-curvature relationships for the brace. Furthermore, the inelastic axial stress-strain relationship of the brace is defined to simulate its nonlinear behavior in tension.

Figs. 3(b and c) respectively show the experimental (Black et al. 1980) and analytical axial force-displacement hysteresis loops for a tubular brace member (TS4×4×1/2) with a slenderness ratio of 80. The brace is subjected to gradually increasing cyclic axial displacements. From the comparison of the Figs. 3(b and c), it is clear that the general characteristics of the hysteresis loop of the analytical model are similar to those of the experimental model. Thus, it is used in the analyses of the CBF to model the nonlinear cyclic behavior of the braces.

Details of the Frames Considered for Analyses

The details of the three frame types considered for NLSP and NLTH analyses are presented in this section. Typical two-story MRF, CBF, and EEDBF are demonstrated in Fig. 1(a). To enable a direct comparison of the performance of the three frames, their member sizes are determined such that all the frames have identical lateral strengths. Additionally, since the design of a MRF is typically controlled by its drift limit (or stiffness), a new frame, MRF*, is designed to have the same code-mandated drift limit per AISC (2002) seismic design provisions as that of the CBF and EEDBF under the same seismic loading. This new frame (MRF*) will allow the comparison of the seismic responses of the frames based on their drift limit (or stiffness) rather than their strength.

For the single-story studies, a typical frame for NLSP analyses (Table 1) and three sets of frames, MRF/CBF/EEDBF 1, 2, and 3 for NLTH analyses (Table 1) are considered to study the effect of the brace contribution to the lateral strength and brace slenderness ratio on the seismic response of the frames. In CBF/EEDBF 1, the brace contribution to the lateral strength of the frames is 40% and the slenderness ratio of the braces is 96. In CBF/EEDBF 2 and 3, the braces resist 60% of the lateral load applied to the frames and the slenderness ratios of the braces are 96 and 125, respectively. MRF 1, 2, and 3 are designed to have the same lateral strength as the corresponding CBF/EEDBF 1, 2, and 3 for a fair comparison of their seismic response within each frame set. Additionally, a MRF* is designed to have the same code-mandated design drift limit as that of the CBF/EEDBF 1, and is used for the comparison of its seismic response with those of MRF/CBF/EEDBF 1. All frames are designed to exhibit nonlinear behavior under moderate to large intensity ground motions (A_p=0.35g and 0.5g).

For the multiple-story studies, two-, four-, and eight-story MRF, CBF, EEDBF, and MRF* are considered. First, the eight-story frame is configured such that each two-story level has the same member sizes, the lateral strength of the frame gradually decreases at the higher-story levels, and the frame exhibits nonlinear behavior under moderate to high intensity ground motions. The two- and four-story frames are then assumed to form the bottom two and four stories of the eight-story frame, respectively. This was done to ensure comparable base shear capacities for all frames to study the effect of the number of stories on the seismic performance of the frames. Furthermore, the frames are designed such that the lateral strength of each story is nearly identical for the MRF, CBF, and EEDBF. Additionally, a new set of multiple-story frames, MRF*, are designed to have the same code-mandated drift limit per AISC (2002) seismic design provisions as that of the CBF and EEDBF under the same seismic loading, to

Table 1. Member Sizes in Single- and Multiple-Story Frames Used for NLSP and NLTH Analyses

Analysis	Frame	Story	Beam	Column	Brace	Shear element
NLSP	MRF	Single	W610×174	W610×195	NA	NA
	CBF / EEDBF	Single	W310×129	W310×174	HSS127×127×6	HP310×110
NLTH	MRF 1	Single	W460×158	W460×193	NA	NA
	MRF 2	Single	W310×143	W360×179	NA	NA
	MRF 3	Single	W310×118	W310×129	NA	NA
	MRF*	Single	W610×113	W690×170	NA	NA
	CBF/EEDBF 1	Single	W310×129	W310×158	HSS127×127×6	HP250×85
	CBF/EEDBF 2	Single	W310×97	W310×118	HSS127×127×6	HP250×62
	CBF/EEDBF 3	Single	W310×45	W310×52	HSS102×102×8	HP250×62
NLTH	MRF	1,2	W460×158	W460×193	NA	NA
		3,4	W310×143	W360×179	NA	NA
		5,6	W310×118	W310×129	NA	NA
		7,8	W310×60	W310×74	NA	NA
	MRF*	1,2	W610×113	W690×170	NA	NA
		3,4	W530×101	W690×152	NA	NA
		5,6	W530×82	W610×125	NA	NA
		7,8	W460×52	W530×82	NA	NA
	CBF / EEDBF	1,2	W310×129	W310×158	HSS127×127×6	HP250×85
		3,4	W310×97	W310×118	HSS127×127×6	HP250×62
		5,6	W310×45	W310×52	HSS102×102×8	HP250×62
		7,8	W250×39	W250×45	HSS89×89×6	W200×36

allow for the comparison of the seismic responses of the frames based on their drift limit (or stiffness) rather than their strength. This ensures a fair comparison of their seismic response under the same seismic loading conditions. Table 1 presents the details of the frames. The elastic fundamental periods of the two-, four-, and eight-story frames (MRF, MRF*, CBF, and EEDBF) are, respectively (0.52, 0.45, 0.28, and 0.31 s), (0.84, 0.71, 0.38, and 0.44 s) and (1.54, 1.23, 0.67, and 0.76 s).

Because of the differences in their elastic periods, the frames will not be subjected to identical seismic demands in the initial elastic stage due to the difference in their elastic fundamental periods. However, the fundamental period, like the other inelastic properties of the frames—such as buckling of the braces in a CBF, shear yielding of the SE in an EEDBF, or yielding of the beams in an MRF—is particular to the structural system of the frame. Thus, one should not be concerned about the frames as being subjected to different seismic demands due to the difference in their fundamental periods as long as the frames are subjected to the same ground motions and intensities.

Ground Motions Considered for Analyses

Seismic ground motions are generally characterized by their peak ground acceleration, A_p, to peak ground velocity, V_p, ratios (Dicleli and Buddaram 2006), which represent their dominant frequency and energy content. Ground motions with intense long-duration acceleration pulses have low A_p/V_p ratios, whereas those with high-frequency short-duration acceleration pulses have high A_p/V_p ratios. Consequently, ground motions with various A_p/V_p ratios are considered to assess the performance of the frames for a wide range of ground-motion characteristics. For this purpose, a set of seven ground motions with A_p/V_p ratios ranging between 5.5 and 21.5 s^{-1} are considered (Table 2). The ground motions are scaled to have $A_p=0.20g$, $0.35g$, and $0.50g$, respectively representing small, moderate, and large intensity earthquakes.

Single-Story Frames

Nonlinear Static Pushover Analyses Results

Comparative Performance of MRF, CBF, and EEDBF for Various Brace Slenderness Ratios

The NLSP analyses results, with a comparison of CBF, EEDBF, and MRF for various slenderness ratios of $\lambda=40$, 80, and 120 representing braces with low, intermediate, and high slenderness, are demonstrated in Fig. 4. In addition to these, a hypothetical case is also studied in which the buckling of the braces is prevented. The axial stiffness of the braces is kept constant for all slenderness ratios considered. It is observed that the elastic lateral stiffness of the MRF (77,300 kN/m) is much smaller than those of the EEDBF (104,000 kN/m) and CBF (122,000 kN/m). Thus, it is expected that both CBF and EEDBF will have limited drift, and hence a more desirable performance under the effect of small to moderate intensity earthquakes where buckling of the braces in

Table 2. Earthquake Records Used in the Analyses

Earthquake	Station	A_p (g)	V_p (cm/s)	A_p/V_p (1/s)
San Fernando (1971)	8244 Orion Blvd.	0.13	23.9	5.5
Loma Prieta (1989)	Oakland Outer Wharf	0.22	35.4	6.1
Northridge (1994)	Arleta & Nordhoff Fire Station	0.34	40.4	8.4
Imperial Valley (1940)	El Centro	0.35	32.3	10.6
Northridge (1994)	Santa Monica City Hall	0.37	24.9	14.6
Whitter Narrows (1987)	90079 Downey Birchdale	0.24	13.7	17.4
Parkfield (1966)	Cholame, Shandon	0.24	10.8	21.5

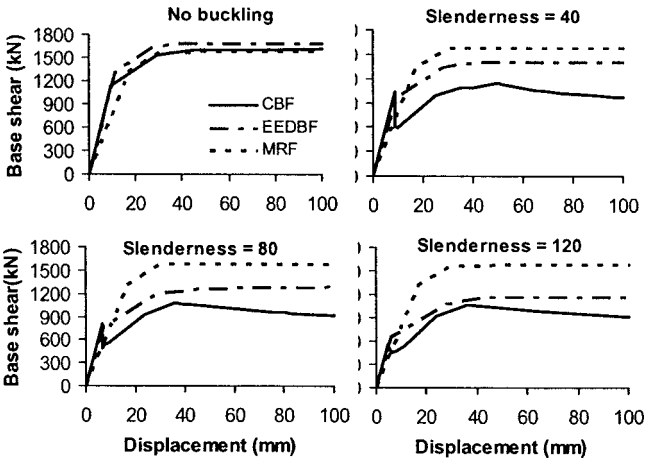

Fig. 4. Base shear versus frame displacement for various brace slenderness ratios

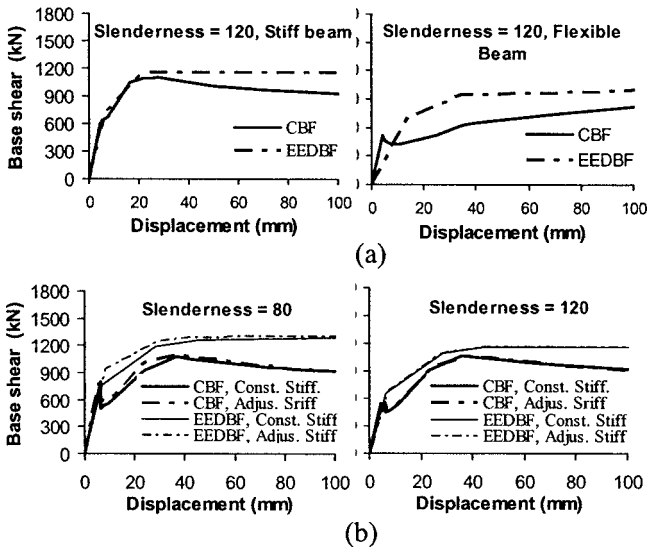

Fig. 5. (a) Effect of beam stiffness on force-displacement response and (b) effect of brace stiffness on the force-displacement response

CBF and yielding of the SE in EEDBF may either be minimal or may not occur. Fig. 4 also demonstrates that the EEDBF has a more stable trilinear lateral force-displacement relationship as compared to CBF for all λ values considered. Moreover, for $\lambda \leqslant 80$, the base shear capacities of the EEDBF and MRF are comparable. This shows that if the EEDBF is designed using braces with low to intermediate slenderness, its monotonic energy dissipating capacity may be comparable to that of an MRF which has much larger member sizes.

Effect of Brace Axial Stiffness

For all the λ values considered above, the axial stiffness of the braces was kept constant. In this section, the effect of using the true axial stiffness of the braces for each specific λ is studied. The true axial stiffness of the braces corresponding to a specific λ is simulated (adjusted) by changing the elastic modulus of steel without altering the length of the braces in the structural model. The analyses results are presented in Fig. 5(b). In the figure, the cases with constant and adjusted brace stiffness are compared. It is observed that the axial stiffness of the brace primarily affects the elastic slope of the force-displacement curve for both CBF and EEDBF. The general behavior of the frames remains nearly unchanged regardless of the axial stiffness of the brace.

Effect of Beam Flexural Stiffness

The performance of the CBF is known to be sensitive to the flexural stiffness of the beam (Khatib et al. 1988). Thus, in this section, the sensitivity of the EEDBF to the stiffness of the beam is studied in comparison to CBF. For this purpose, the flexural stiffness of the beam of the frames considered in the analyses is modified by a factor of 10 to obtain a flexible and a stiff beam. Fig. 5(a) displays a comparison of the lateral force-displacement relationship of the EEDBF and CBF for stiff and flexible beam cases for a brace with $\lambda = 120$. For $\lambda = 120$, the buckling load is very small compared to the tensile yield force of the brace. Consequently, in the case of the CBF, a large unbalanced vertical load will be produced on the beam due to the difference between the vertical components of the axial loads in the tension and compression braces. Thus, the flexible beam may be forced to displace down and may eventually reach its flexural yield capacity. This phenomenon produces a faster reduction in the axial load capacity of the compression brace (Khatib et al. 1988), and hence a reduction in the lateral load capacity of the CBF compared to the stiff beam case as observed from Fig. 5(a). In the case of the EEDBF, the flexural stiffness of the beam affects only the elastic stiffness of the frame and the magnitude of the lateral displacement at which the ultimate strength of the frame is reached. For the flexible beam case, the lateral stiffness of the SE in EEDBF is reduced due to the increased rotations at the base of the element resulting from the larger flexibility of the beam. As a result, the elastic stiffness of the EEDBF becomes smaller and the lateral displacement at the ultimate strength level of the frame becomes larger. However, the forces in the tension and compression braces of the EEDBF remain identical due to the controlled yielding of the SE prior to buckling of the compression brace. This results in a zero unbalanced vertical force on the beam. Consequently, a more stable behavior is observed in the case of the EEDBF regardless of the beam stiffness.

Nonlinear Time-History Analyses Results

Performance of the Frames versus Intensity and Frequency Characteristics of Ground Motions

Fig. 6(a) displays the maximum story drifts of the MRF (and MRF* for Frame Set 1), CBF, and EEDBF for each frame set as a function of the A_p/V_p ratio of the ground motions for low ($A_p = 0.20g$), medium ($A_p = 0.35g$), and high ($A_p = 0.50g$) intensities respectively.

For $A_p = 0.20g$ and $0.35g$, Fig. 6(a) shows that while the lateral drift responses of the CBF and EEDBF are comparable, the MRF (and MRF* for Frame Set 1) produces higher drifts for the range of A_p/V_p ratios and for all frame sets considered. It is also observed that while the peak drifts for the MRF occur at low to intermediate A_p/V_p ratios, those for the MRF*, CBF, and EEDBF are generally more uniform.

For $A_p = 0.5g$, there is a considerable increase in the value of lateral drifts of the frames, especially in the cases of the MRF and CBF. For Frame Sets 1, 2, and 3, the peak drifts of the MRF, CBF, and EEDBF (and MRF* for Frame Set 1 only) are, respectively (47.1, 33.4, 20.8, and 26.3 mm), (66.8, 224.4, and 21.3 mm), and (61.8, 273.8, and 21.4 mm), for the range of A_p/V_p ratios considered. It is also observed that while the MRF, MRF*, and EEDBF

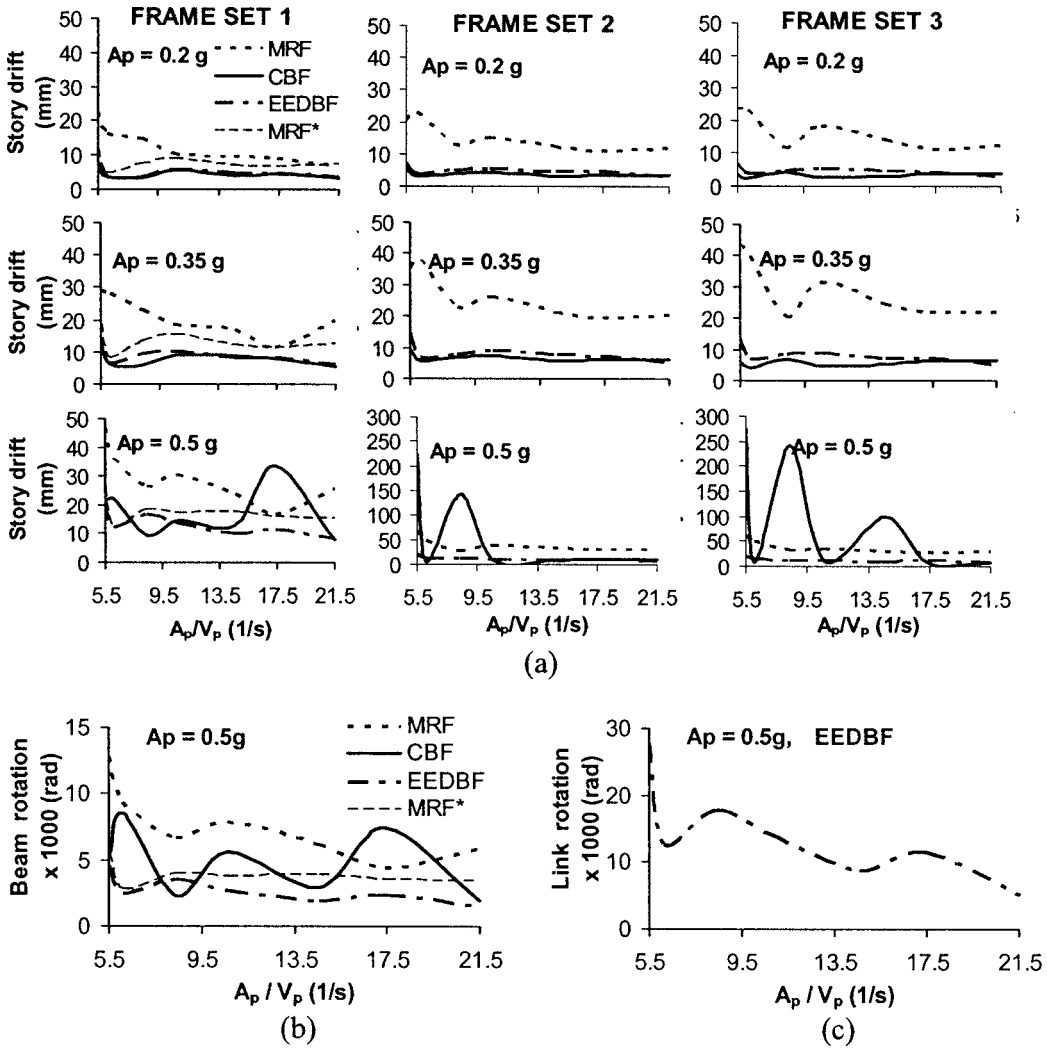

Fig. 6. (a) Maximum story drift versus A_p/V_p ratio of the ground motions for the three frame sets and for various A_p; (b) beam-end rotations versus A_p/V_p for Frame Set 1; and (c) link rotation versus A_p/V_p for the EEDBF in Frame Set 1

display a relatively uniform response over the range of A_p/V_p ratios and ground-motion intensities considered, CBF seems to be highly sensitive to the frequency characteristics (A_p/V_p ratio) of the ground motion. A close examination of the behavior of the CBF revealed that the sensitivity of the frame's seismic response to the A_p/V_p ratio of the ground motion mainly depends on the buckling behavior of the brace. For ground motions with lower intensities, either no buckling or limited buckling behavior of the brace is observed. This results in a more uniform response of the frame over the range of A_p/V_p ratios of the ground motions considered. However, for ground motions with higher intensities, the buckling behavior of the brace becomes more dominant, and the frame becomes more sensitive to the A_p/V_p ratio due to the degradation in the stiffness and strength of the frame associated with the buckling phenomenon.

The performance of the frames within Frame Set 1 is also measured by comparing the beam-end rotations in Fig. 6(b). It is observed that the EEDBF exhibits smaller beam-end rotations compared to all the other frames. Furthermore, the shear rotation of the SE of the EEDBF is plotted as a function of the A_p/V_p ratio in Fig. 6(c). The shear strain is observed to be less than 0.04 radians. Based on the stiffener spacing calculations using Eq. (3), the SE may be able to accommodate such a shear rotation without the need for stiffeners.

In summary, both the CBF and EEDBF display a more desirable response than that of the MRF and MRF* for low to medium intensity ground motions over the range of A_p/V_p ratios considered. However, for high intensity ground motions, the response of the CBF becomes highly unstable due to the effect of brace buckling. The EEDBF displays a highly stable response for the range of A_p/V_p ratios considered. The story drift of the EEDBF is the smallest of all frames considered in this study.

Effect of Brace Contribution and Slenderness

In this section, the effect of the brace slenderness and contribution to the lateral strength of the frame on the seismic response of the EEDBF and CBF are investigated in relation to MRF.

Fig. 6(a) demonstrates that for A_p=0.20g and 0.35g, the EEDBF generally yields a response comparable to that of the CBF regardless of the properties of the frame for the range of brace contribution (40%–60%) and brace slenderness ratios (96 and 125) considered. Obviously, since the brace contribution

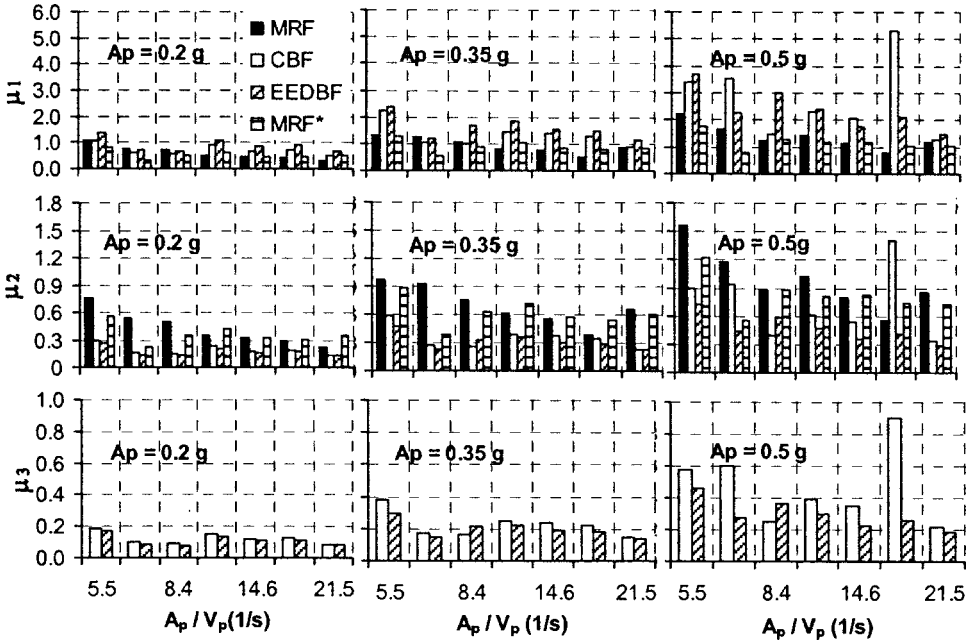

Fig. 7. Ductility ratios as a function of A_p/V_p ratio of the ground motions for various A_p

to the lateral strength is smaller in CBF 1 (40%) the story drift for this frame is larger than those of the other two frames (CBF 2 and 3).

For $A_p=0.5g$, CBF 2 and 3 produce exceptionally higher drifts compared to those of the CBF 1, EEDBF 1, 2, 3, and even MRF 1, 2, 3, and MRF*. This may be attributed to the more dominant buckling behavior of the braces resulting from the larger brace contribution to the lateral strength in CBF 2 and 3. It is also observed that the lateral drift of the CBF 3 is even higher in comparison to that of the CBF 2, due to the presence of braces with larger slenderness ratios. Furthermore, the seismic response becomes more sensitive (unpredictable) to the A_p/V_p ratio of the ground motion for CBF 2 and 3 as observed from the humps and undulations displayed in the two graphs at the bottom right of Fig. 6(a). Moreover, Fig. 6(a) clearly shows that the lateral drift of the EEDBF for low to medium intensity ground motions is smaller than that of the MRF (and MRF* for Frame Set 1) and comparable to that of the CBF for all the frame sets considered. However, for high intensity ground motions, the lateral drift of the EEDBF is considerably smaller than those of all the frames considered at certain A_p/V_p ratios.

In summary, the performance of the CBF is highly dependent on the slenderness and contribution of the brace to the lateral strength of the frame. However, the performance of the EEDBF is more stable and is independent of such parameters. Furthermore, EEDBF yields the smallest drifts of all the frames when subjected to high intensity ground motions. This is indicative of less potential damage to the essential structural members of the EEDBF. This will be formally investigated in the subsequent section.

Potential Seismic Damage to the Single-Story Frames

In this section, the extent of yield penetration into the members of the three frames in Frame Set 1 is studied to compare the possible damage in the plastic zones of the three frames subjected to a potential earthquake. Fig. 7 displays a comparison of the yield penetration into the members of the three frames for different values of A_p in the form of graphs between A_p/V_p and displacement ductility ratios, $\mu_{1=}u_{\max}/u_{y1}$ (top), $\mu_{2=}u_{\max}/u_{y2}$ (middle), and $\mu_{3=}u_{\max}/u_{y3}$ (bottom), where $u_{\max}$ is the maximum frame drift and u_{y1}, u_{y2} and u_{y3} are the drifts corresponding to the sequential yielding of the various components of the frames. For the MRF and MRF*, u_{y1} and u_{y2} correspond to the yielding of the beam and then the columns, respectively; for the CBF, u_{y1}, u_{y2}, and u_{y3} correspond to the yielding of the tension brace, the beam, and then the columns respectively; and for the EEDBF, u_{y1}, u_{y2}, and u_{y3} correspond to the yielding of the SE, the beam, and then the columns, respectively. Ductility ratios larger than 1.0 are indicative of yielding and thus, potential damage to the plastic zones of the frame components. It is noteworthy that for the MRF and EEDBF, the design of the frames are performed such that ductility ratios larger than 1.0 are obtained in the beams for the MRF and in the SEs for the EEDBF. These specific elements are expected to experience large inelastic deformations or ductilities to effectively dissipate the earthquake input energy without the collapse of the structure. Therefore, large ductilities are indicative of efficient dissipation of earthquake input energy. However, large ductilities are achieved at the expense of damage in plastic hinge zones as demonstrated by Bruneau et al. (1998) even for the beams of MRFs exhibiting stable hysteretic behavior. The extent of damage in the plastic zones is proportional to the magnitude of the ductility ratio. For instance, if the ductility ratio is smaller than 1.0, then the structure remains elastic, and hence experiences no yielding and associated damage.

The set of three graphs at the top of Fig. 7 demonstrates that for small intensity ground motions ($A_p=0.20g$), the frames generally remain within the elastic limit ($\mu_1 \leqslant 1$). However, at medium to large intensity ground motions ($A_p=0.35g$ and $0.50g$), yielding of the frame members is observed ($\mu_1 \geqslant 1$). That is, the braces in the CBF have buckled and yielded, flexural yielding of the beams in the MRF and MRF* have occurred, and the SE in the EEDBF has yielded in shear. Fig. 7 also reveals that μ_1 of the MRF and MRF* is smaller than those of the other two frames. This is mainly due to the higher u_{y1} of the MRF and MRF* compared to those of the others due to the large flexibilities of the frames. The second row of graphs from the top of Fig. 7 shows

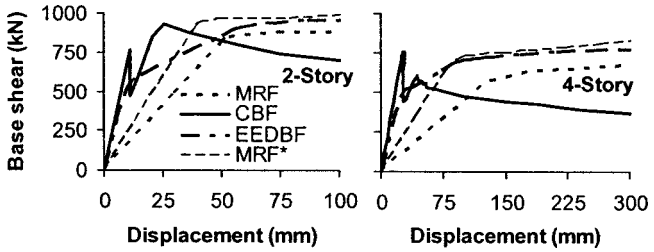

Fig. 8. Base shear versus top displacement for two- and four-story frames

that for some A_p/V_p ratios, limited yield penetration ($\mu_2 \geq 1$) into the columns of the MRF and MRF* (less yielding in the case of the MRF*) has occurred for medium to large intensity ground motions. For high intensity ground motions, yielding of the beam in the CBF is also observed ($\mu_2 \geq 1$). However, for the EEDBF—since $\mu_2 \leq 1$ for the range of A_p/V_p ratios considered—no member other than the SE experienced any yielding.

The set of three graphs at the bottom of Fig. 7 reveals that $\mu_3 < 1.0$ for the range of A_p/V_p ratios considered. Thus, no yield penetration into the columns of both frames is observed. However, it is worth mentioning that for $A_p=0.50g$, μ_3 ranges between 0.22 and 0.91 for the CBF and 0.18 and 0.46 for the EEDBF. This clearly indicates that the EEDBF has a larger lateral drift reserve capacity before the yielding of the columns can possibly take place. Thus, in the case of a potential high intensity earthquake, the EEDBF is less likely to experience any significant damage to the gravity load carrying structural components of the frame (beams and columns) compared to CBF, MRF, and MRF*.

Multiple-Story Frames

Nonlinear Static Pushover Analyses Results

NLSP analyses of the multiple-story frames are performed assuming a triangular lateral load pattern along the height of the frames. The results of the NLSP analyses of the two- and four-story frames are depicted in Fig. 8. The figure displays the base shear force as a function of the drift at the top story level. In the case of the CBF, the loss of lateral strength associated with buckling behavior is clearly observed. For the two-, four-, and eight-story CBF, the braces below the first-, third-, and fifth-story levels exhibited the first buckling behavior, respectively. In all cases, the elastic stiffness of the MRF and MRF* is lower than those of the other two frames, and the frames reached their ultimate lateral strength at a higher drift value. On the other hand, the EEDBF exhibits a higher elastic stiffness compared to MRF and MRF*, as well as a more stable monotonic force-deformation relationship compared to CBF. The observations from the NLSP analyses of multiple-story frames confirm the findings from the one-story studies.

Nonlinear Time-History Analyses Results

Performance of Multiple-Story Frames in Relation to Frequency Characteristics and Intensity of Ground Motions

Fig. 9(a) displays the maximum interstory drifts of the MRF, MRF*, CBF, and EEDBF for two-, four-, and eight-story frames as a function of the A_p/V_p ratio of the ground motions considered for low ($A_p=0.20g$), medium ($A_p=0.35g$), and high ($A_p=0.50g$) intensities, respectively.

For $A_p=0.20g$ and $0.35g$, Fig. 9(a) shows that while the seismic lateral displacement responses of the CBF and EEDBF are comparable for the two- and four-story frames, the MRF and MRF* produce higher drifts for the range of A_p/V_p ratios considered. In the case of the eight-story frames, while the CBF and MRF exhibit comparable interstory drifts, the EEDBF and MRF* produce lower interstory drifts. It is also observed that while the peak drifts for the MRF and MRF* generally occur at low to intermediate A_p/V_p ratios, those for the CBF and EEDBF are generally more uniform.

For $A_p=0.5g$, there is a considerable increase in the interstory drifts of the frames, especially in the case of the MRF and CBF. The dramatic increase in the interstory drifts of the CBF is due to the buckling of the braces resulting in soft-story formations. It is also observed that while both the MRF, MRF*, and EEDBF display relatively stable responses over the range of A_p/V_p ratios and ground-motion intensities considered, CBF seems to be highly sensitive to the A_p/V_p ratio of the ground motion at higher ground-motion intensities due to the buckling of the braces.

The performance of the frames is also measured by comparing the beam-end rotations in Fig. 9(b) for the four-story frames. It is observed that the EEDBF exhibits smaller beam end rotations compared to all other frames. Furthermore, the shear rotation of the SE of the four-story EEDBF is plotted as a function of the A_p/V_p ratio in Fig. 6(c). For most cases, the shear rotation is observed to be less than 0.04 radians. Based on the stiffener spacing calculations using Eq. (3), the SE may be able to accommodate such a shear strain without the need for stiffeners.

In summary, both the CBF and EEDBF display a stable and a more desirable response than that of the MRF and MRF* for low to medium intensity ground motions for two- and four-story frames over the range of A_p/V_p ratios considered. However, for high intensity ground motions and for an increasing number of stories, the response of the CBF becomes highly unstable due to the effect of brace buckling. The EEDBF and MRF* display a stable response for the range of A_p/V_p ratios considered.

Displacement Profile of the Frames

Fig. 10 compares the deformed shapes of the two-, four-, and eight-story CBF, MRF, MRF*, and EEDBF for a ground motion with $A_p/V_p=8.4\ s^{-1}$ scaled for $A_p=0.2g$, $0.35g$, and $0.5g$. The deformed shapes of the frames are obtained at the instant when the maximum interstory drift occurs.

For $A_p=0.2g$ and $0.35g$, the figure reveals that for the two- and four-story frames, both the CBF and EEDBF display similar deformed shapes. The deformation of both frames is mostly concentrated at the first-story level with the deformation at the upper story levels being relatively modest. In the case of the MRF and MRF*, the deformation at the first-story level is also large. However, the MRF and to some extent the MRF*, also experience notable deformations at the upper story levels due to the flexibility of the frames. For $A_p=0.5g$, the buckling of the braces in the two- and four-story CBF dominates the behavior of the frame, where interstory drifts larger than those of the EEDBF are observed. The MRF and MRF* to a lesser extent, also experience deformations larger than those of the EEDBF due to the larger flexibility of the frames and yielding of the beams. The EEDBF generally exhibits a more stable lateral deformation pattern for the range of ground-motion intensities considered.

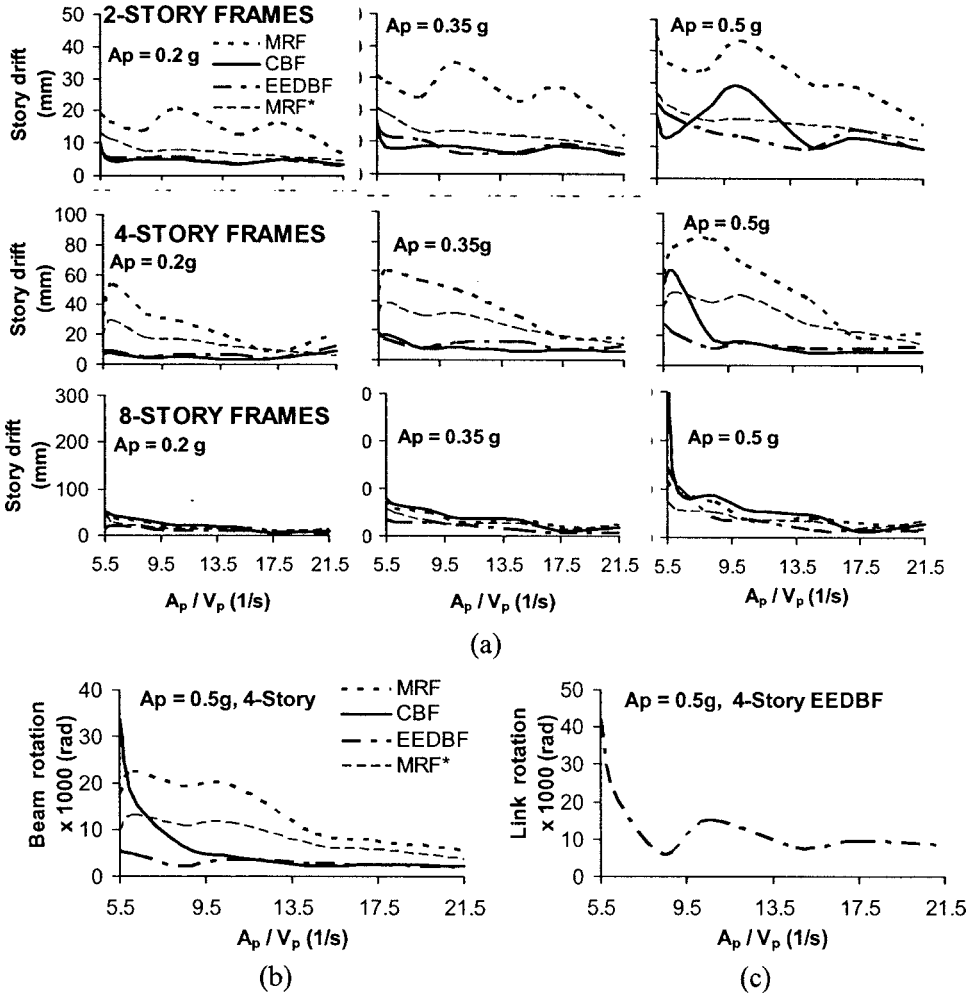

Fig. 9. (a) Maximum interstory drift versus A_p/V_p ratio of the ground motions for various A_p for the two-, four- and eight-story frames; (b) beam-end rotations versus A_p/V_p for the four-story frames; and (c) link rotation versus A_p/V_p for the four-story EEDBF

For the eight-story frames, the buckling of the braces dominates the behavior of the CBF for the range of ground-motion intensities considered. This resulted in soft-story formations, as observed from Fig. 10, and the concentration of the energy dissipation at the intermediate-story levels. It is also observed that the displacement profile of the CBF is highly sensitive to the A_p/V_p ratio of the ground motion and the number of stories. Consequently, the design of the CBF becomes highly unreliable. Compared to CBF, the MRF and MRF* exhibit a better lateral deformation pattern, and hence a more even distribution of energy dissipation along the height of the frame. Nevertheless, the EEDBF exhibits even a more uniform lateral displacement profile and a smaller interstory drifts compared to the other frames for all ground-motion intensities considered.

Effect of Number of Stories on the Seismic Response of the Frames

In this section, the analyses results for the multistory frames are consolidated, and the average of the maximum interstory drifts from the seven earthquakes are presented in the form of bar charts for two-, four-, and eight-story frames corresponding to low, medium, and high intensities in Fig. 11. The figure reveals that for two- and four-story frames, the MRF and MRF* yield higher interstory drifts than those of the CBF and EEDBF due to the flexibility of the frames and yielding of the beams. Generally, the CBF displays a reasonably good response at low and moderate intensities of ground motions and for a smaller number of stories. However, for a larger number of stories, a sudden increase in the interstory story drifts of the CBF is observed, indicating an unstable behavior. The presence of more slender braces and flexible beams at the upper stories promotes the buckling of the braces. This results in a loss of lateral stiffness of the frame, and hence larger interstory drifts with an increasing number of stories. EEDBF, on the other hand, exhibits a more uniform increase of the interstory drift as the height of the frame increases, indicating a more desirable and reliable response compared to the CBF. Furthermore, the EEDBF is observed to generally have a smaller interstory drift that is indicative of less potential structural and nonstructural seismically induced damage compared to the other frames.

Damage Analyses of Multiple-Story Frames

In this section, damage analyses of the three frames are performed to further assess the performance of the proposed EEDBF in relation to CBF and MRF.

Seismic damage quantification is generally represented by damage indices that range between 0 (no damage) and 1 (complete collapse). Many researchers have proposed a number of damage models that calculate damage indices (Banon et al. 1981;

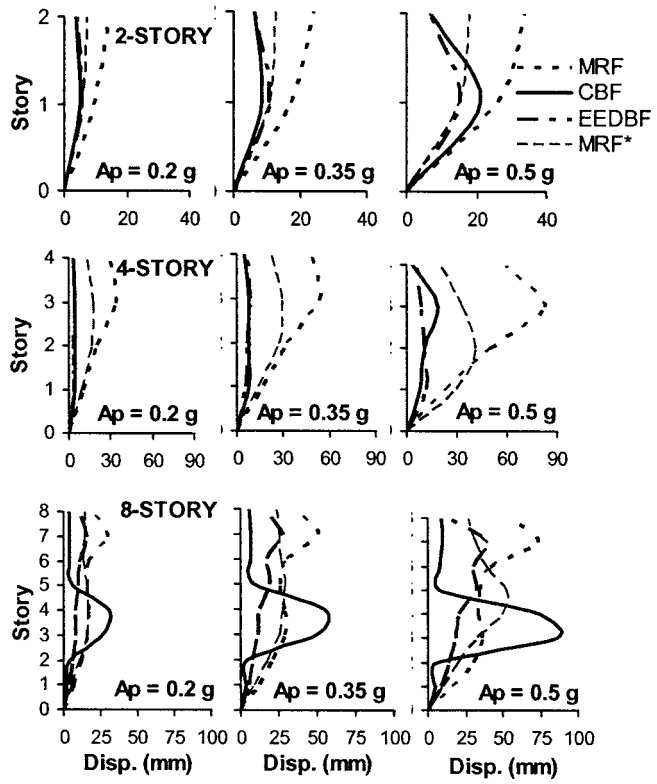

Fig. 10. Displacement profile of the two-, four-, and eight-story frames for various A_p (A_p/V_p=8.4 s^{-1})

Park and Ang 1985; Kunnath et al. 1997; Chai 1999; Perera et al. 2000; Mehanny and Deierlein 2001; Khashaee 2005). However, most of these damage models have concentrated almost exclusively on flexural modes of failure. Thus, they may not be applicable to the EEDBF and CBF due to the presence of shear yielding and brace buckling. Nevertheless, the damage model proposed by Hindi and Sexsmith (2001) is primarily based on the monotonic energy dissipating capacity of structural elements before and after the application of reversed cyclic loading. Therefore, it may be universally applicable to structural members exhibiting failure modes other than flexure, including steel members failing in the shear or buckling mode. Furthermore, it is different than most existing damage models in that it does not require any tuning of damage equation coefficients for a particular type of failure. Consequently, it is used for the damage assessment of the frames considered in this study.

Damage Model of Hindi and Sexsmith (2001)

The damage model takes as a reference the monotonic energy dissipation capacity of a structure in the undamaged virgin state, which is defined as the area, A_o, under the static pushover curve up to the point of failure [Fig. 12(a)]. With the actual "n" cycles of load-displacement history applied on the structure due to a potential earthquake, the remaining monotonic energy dissipation capacity of the structure, compared to that in its virgin state, defines the extent of damage. The remaining monotonic energy dissipation capacity of the structure is defined as the area, A_n, under the static pushover curve obtained from the end of the last cycle, n, to the failure point [Fig. 12(b)]. Accordingly, the damage index is the ratio

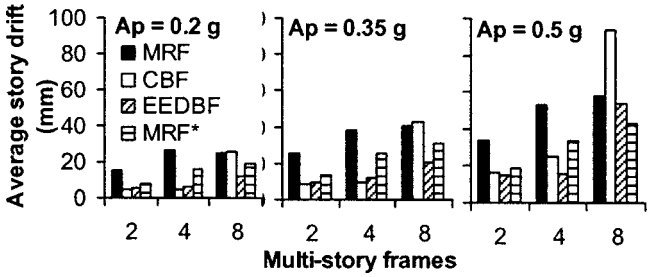

Fig. 11. Average of maximum interstory drifts as a function of the number of stories for various A_p

$$D_n = \frac{(A_o - A_n)}{A_o} \tag{6}$$

A damage index of 0 (A_n=A_o) is indicative of no damage, whereas a damage index of 1 (A_n=0) is indicative of complete damage or collapse.

Damage Analyses of the Frames

The damage analyses of the MRF, MRF*, CBF, and EEDBF are performed on four-story frames. NLSP analyses results of Fig. 8 are used to obtain the monotonic energy dissipation capacity, A_o, in the virgin state. The failure point is assumed as the displacement corresponding to the FEMA prescribed story drift limits (FEMA 2000a). The frames are then subjected to two ground motions with A_p/V_p=5.5 and 8.4 s^{-1} scaled to represent moderate (A_p=0.35g) and high (A_p=0.5g) intensity earthquakes. At the end of the seismic event, the properties of the frames are different from the original state, as the frames undergo permanent plastic deformation and suffer a reduction in the lateral stiffness and strength values. Displacement controlled NLSP analyses are then performed on the frames starting from the end of the last cycle of the load-displacement curve due to the applied earthquake ground motion. The area (energy) under the static pushover curve, A_n, is then calculated for the damaged state and substituted in Eq. (6) to obtain the damage indices for the frames.

Discussion of Damage Analyses Results

The results of the damage analyses of the frames are presented in Table 3. It is observed that earthquakes with a low A_p/V_p ratio and high intensity are particularly damaging to CBF, as it loses up to 40% of its monotonic energy absorption capacity due to the buckling of the braces. The MRF and, to a lesser extent, MRF* display small to moderate damage indices for the A_p/V_p ratios and intensities considered in the analyses. On the other hand, EEDBF

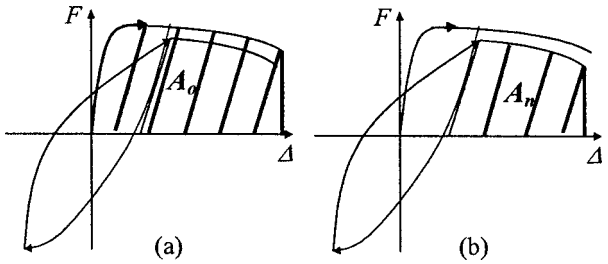

Fig. 12. Definition of damage equation parameters of the model by Hindi and Seximith (2001): (a) monotonic energy in the virgin state; (b) monotonic energy after the application of load-displacement cycles

Table 3. Damage Indices for the Four-Story MRF, MRF*, CBF, and EEDBF

		A_p/V_p=5.5 s^{-1}				A_p/V_p=8.4 s^{-1}			
		A_p=0.35g		A_p=0.5g		A_p=0.35g		A_p=0.5g	
Frame	A_o (kN m)	A_n (kN m)	D_n	A_n (kN m)	D_n	A_n (kN m)	D_n	A_n (kN m)	D_n
MRF	129.1	103.2	0.201	86.5	0.330	123.8	0.042	114.3	0.115
MRF*	200.9	184.2	0.083	173.4	0.137	195.6	0.026	180.5	0.102
CBF	87.5	75.7	0.135	51.8	0.408	79.4	0.094	74.3	0.151
EEDBF	133.7	124.8	0.066	119.9	0.103	129.7	0.030	128.8	0.036

has generally lower damage indices compared to the other frames. This indicates a greater reserve energy dissipation capacity, less damage, and smaller rehabilitation cost after a major seismic activity. Thus, the damage analyses of the frames further reinforce the more desirable behavior of the EEDBF, as compared to the conventional frames.

Conclusions

The seismic performance of the proposed EEDBF is investigated analytically in comparison to MRF, MRF*, and CBF through NLSP, NLTH, and damage analyses using single- and multiple-story frames. The conclusions derived from this study are presented next.

The NLSP analyses results revealed that the proposed EEDBF shows a more desirable behavior compared to the conventional frames considered in this study. The EEDBF exhibits a more stable lateral force-displacement relationship compared to that of the CBF, as no degradation in the lateral strength is observed due to the buckling of the braces. Moreover, although the EEDBF has a higher elastic stiffness and smaller member sizes compared to MRF, its monotonic energy dissipation capacity is comparable to that of the MRF for low and intermediate brace slenderness values. Thus, while the EEDBF combines the advantages of both frames, it eliminates most of the disadvantages particular to each frame.

The NLTH analyses of the MRF, MRF*, CBF, and EEDBF revealed that MRF and MRF* generally yield large interstory drifts for small to medium intensities of ground motions compared to the other two frames due to their larger flexibility. The penetration of plastic deformation into the members of the MRF and, to a lesser extent, MRF* is also generally larger compared to the EEDBF (although the drifts of the MRF* are more comparable to those of the EEDBF). On the other hand, CBF generally displays a good response for low to moderate intensity ground motions and for a lower number of stories. Nonetheless, for high intensity ground motions and for a larger number of stories, a sudden deterioration in the strength and stiffness of the frame is observed due to the effect of brace buckling. This resulted in soft-story formations and considerable plastic penetration into the essential structural components of the CBF. Furthermore, the behavior of the CBF is found to be highly dependent on the brace contribution to the overall strength of the frame, the slenderness of the braces, and the A_p/V_p ratio of the ground motion. On the other hand, EEDBF displays a more stable behavior over a wide range of structural and ground-motion properties. It also exhibits a more even distribution of earthquake input energy over the height of the frame, and generally yields lower drifts for a wide range of A_p/V_p ratios and intensities of ground motions as compared to the other frames studied. Moreover, the behavior of the EEDBF is independent of the brace contribution to the lateral strength of the frame and the slenderness of the braces. Thus, EEDBF combines the advantages of both CBF and MRF; and therefore, displays an overall more desirable behavior as compared to the other frames.

Damage analyses of the frames revealed that the EEDBF generally exhibits less damage and a larger reserve lateral deformation capacity compared to CBF and MRF (and MRF*). Thus, in the event of a potential earthquake, it is anticipated that the yielding of the SE in the EEDBF will prevent buckling of the braces and minimize damage to the essential structural components of the frame. It is anticipated that the damaged SE can be easily replaced for a relatively small cost. This may result in a minimal postearthquake rehabilitation cost compared to the other frames.

References

ADINA. (2004). *Automatic dynamic incremental nonlinear analysis, version 8.2*, ADINA R&D, Inc., Watertown, Mass.

AISC. (2001). *Manual of steel construction, load, and resistance factor design*, American Institute of Steel Construction, Chicago.

AISC. (2002) "Seismic provisions for structural steel buildings." *ANSI/AISC 341-02*, American Institute of Steel Construction, Chicago.

Banon, H., Irvine, H. M., and Biggs, J. M. (1981). "Seismic damage in reinforced concrete frames," *J. Struct. Div.*, 107(9), 1713–1729.

Black, G. R., Wenger, B. A., and Popov, E. P. (1980). "Inelastic buckling of steel struts under cyclic load reversals," *Rep. No. UCB/EERC-80/40*, Earthquake Engineering Research Center, Univ. of California, Berkeley, Calif.

Bruneau, M., Uang, C. M., and Whittaker, A. (1998). *Ductile design of steel structures*, McGraw-Hill, New York.

Chai, Y. H. (1999). "Characterization of story-level seismic damage using an energy-based damage model." *Exp. Mech.*, 39(1), 53–61.

Chen, C.-C., Chen, S.-Y., and Liaw, J.-J. (2001). "Application of low yield strength steel on controlled plastification ductile concentrically braced frames." *Can. J. Civ. Eng.*, 28(5), 823–836.

Clark, P., Aiken, I., Kasai, K., Ko, K., and Kimura, I. (1999). "Design procedures for building incorporating hysteretic damping devices." *Proc., 68th Annual Convention of the Structure Engineers Associate of California*, Santa Barbara, Calif.

Della Corte, G., De Matteis, G., Landolfo, R., and Mazzolani, F. M. (2002). "Seismic analysis of MR steel frames based on refined hysteretic models of connections." *J. Constr. Steel Res.*, 58(10), 1331–1345.

Dicleli, M., and Albhaisi, S. M. (2004). "Effect of cyclic thermal loading on the performance of steel H piles in integral bridges with stub-abutments." *J. Constr. Steel Res.*, 60(2), 161–182.

Dicleli, M., and Buddaram, S. (2006). "Effect of isolator and ground motion characteristics on the performance of seismic-isolated bridges." *Earthquake Eng. Struct. Dyn.*, 35(2), 233–250.

Dicleli, M., and Mehta, A. (2007). "Simulation of inelastic cyclic buckling behavior of steel box sections." *Comput. Struct.*, 85(7–8), 446–457.

FEMA. (2000a). "NEHRP recommended provisions for the development of seismic regulations for new buildings and other structures." *BSSC 2000*, Washington, D.C.

FEMA. (2000b), "Prestandard and commentary for the seismic rehabilitation of buildings." *FEMA 356*, Washington D.C.

Georgescu, D., Toma, C., and Gosa, O. (1992). "Postcritical behavior of 'K' braced frames." *J. Constr. Steel Res.*, 21(1), 115–133.

Gwozdz, M., and Machowski, A. (1997). "Strengthening of building steel frames by modification of structural system." *Arch. Civ. Eng.*, 43(1), 37–49.

Hjelmstad, K. D., and Popov, E. P. (1983). "Cyclic behavior and design of link beams." *J. Struct. Eng.*, 109(10), 2387–2403.

Hindi, R. A., and Sexsmith, R. G. (2001). "A proposed damage for RC bridge columns under cyclic loading." *Earthquake Spectra*, 17(2), 261–289.

Kasai, K., and Popov, E. P. (1986a). "General behavior of WF steel shear link beams." *J. Struct. Eng.*, 112(2), 362–382.

Kasai, K., and Popov, E. P. (1986b). "Cyclic web buckling control for shear link beams." *J. Struct. Eng.*, 112(3), 505–523.

Khashaee, P. (2005). "Damage-based seismic design of structures." *Earthquake Spectra*, 21(2), 371–387.

Khatib, I. F., Mahin, S. A., and Pister, K. S. (1988). "Seismic behavior of concentrically braced steel frames." *Rep. No. UCB/EERC-88/01*, Earthquake Engineering Research Center.

Kunnath, S. K., EL-Bahy, A., Taylor, A., and Stone, W. (1997). "Cumulative seismic damage of reinforced concrete bridge piers." *NCEER Rep. No. 97-0006*, State Univ. of New York, Buffalo, N.Y.

McDaniel, C. C., Uang, C.-M. U., and Seible, F. (2003). "Cyclic testing of built-up steel shear inks for the New Bay Bridge." *J. Struct. Eng.*, 129(6), 801–809.

Mehanny, S. S. F., and Deierlein, G. G. (2001). "Seismic damage and collapse assessment of composite moment frames." *J. Struct. Eng.*, 127(9), 1045–1053.

Okazaki, T., Arce, G., Ryu, H.-C., and Engelhardt, M. D. (2005). "Experimental study of local buckling, overstrength, and fracture of links in eccentrically braced frames." *J. Struct. Eng.*, 131(10), 1526–1535.

Park, C. H., Lee, D. G., and Kim, J. K. (1997). "Effect of gravity load on seismic response of steel-framed structures." *Eng. Struct.*, 19(6), 439–451.

Park, Y. J., and Ang, A. H.-S. (1985). "Mechanistic seismic damage model for reinforced concrete." *J. Struct. Eng.*, 111(4), 722–739.

Perera, R., Carnicero, A., Alarcon, E., and Gomez, S. (2000). "Fatigue damage model for seismic response of RC structures." *Comput. Struct.*, 78(1), 293–302.

Perotti, F., and Scarlassara, G. P. (1991). "Concentrically braced frames under seismic actions: Nonlinear behavior and design coefficients." *Earthquake Eng. Struct. Dyn.*, 20(5), 409–427.

Phocas, M. C., and Pocanschi, A. (2003). "Steel frames with bracing mechanism and hysteretic dampers." *Earthquake Eng. Struct. Dyn.*, 32(5), 811–825.

Rai, D. C., Goel, S. C. (2003). "Seismic evaluation and upgrading of chevron braced frames." *J. Constr. Steel Res.*, 59(8), 971–994.

Redwood, R. G., and Channagiri, V. S., (1991). "Earthquake resistant design of concentrically braced steel frames." *Can. J. Civ. Eng.*, 18(5), 839–850.

Roeder, C. W. (1989). "Seismic behavior of concentrically braced frame." *J. Struct. Eng.*, 115(8), 1837–1855.

Sam, M.-T., Balendra, T., and Liaw, C.-Y. (1995). "Earthquake-resistant steel frames with energy dissipating knee elements." *Eng. Struct.*, 17(5), 334–343.

Tremblay, R., and Robert, N. (2001). "Seismic performance of low- and medium-rise chevron braced steel frames." *Basin Res.*, 28(4), 699–714.